Cumhuriyet Science Journal
e-ISSN: 2587-246X
ISSN: 2587-2680
Cumhuriyet Sci. J., 41(2) (2020) 506-520
http://dx.doi.org/10.17776/csj.632197

Comparison of functionally graded and ungraded cylinder liners with finite element analysis

Fatih CİVELEK [1], **Cem ERTEK** [1,*]

[1]*Department of Manufacturing Engineering, Sivas Cumhuriyet University, 58140 Sivas/ TURKEY*

Abstract

In this study, functionally graded and ungraded Al-Si cylinder liners have been compared by the finite element analysis. At the beginning of the study, the most sold gasoline-powered automobiles in recent years have been investigated and the dimensions of the Al-Si cylinder liner have been determined. Al-Si alloy based cylinder liners with a wall-thickness of 6 mm and inner diameter of 74 mm, an outer diameter of 86 mm and a length of 165 mm have been designed. The functionally graded cylinder liner has a twenty-layered structure, and the silicon content of each layer is distinct. Si contents on the inner and the outer surfaces of the functionally graded liner are 32 vol.% and 8.5 vol.%., respectively. The ungraded cylinder liner, on the other hand, has a homogeneous structure and the silicon content of 21 vol.%. The maximum Von Mises stresses reached as a result of thermal loads in the functionally graded and ungraded cylinder liners are determined to be 47.526 MPa and 95.951 MPa, respectively. It has been observed that maximum Von Mises stress decreases by approximately 50% thanks to the functional grading.

Article info

History:
Received: 12.10.2019
Accepted: 27.05.2020
Keywords: Functionally graded material, Finite element method, Al-Si alloys, Thermal stresses.

1. Introduction

Nowadays as an alternative to cast iron, Al-Si alloys are increasingly used to manufacture engine parts. In addition to having a high strength to weight ratio, Al-Si alloys also have excellent thermal conductivity property which is necessary to remove the heat released by combustion [1]. The applications of Al-Si alloys in the automotive industry include engine parts, in particular, cylinder liners, and engine blocks. The use of these alloys reduces engine weight, exhaust gas emissions and fuel consumption [2].

The use of engine blocks made of hypereutectic Al-Si alloy has been contemplated by many companies. Al17Si4CuMg alloy casting to produce cylinder block is a very difficult and expensive process, therefore low-priced hypoeutectic Al-Si alloys are used to manufacture engine blocks. The tribological characteristics of these alloys cannot provide the properties necessary for the combustion chamber surface. Surface coating or use of cylinder liner is required in order to solve this problem [2]. The surface of the cylinder can be coated with Ni/SiC (Nikasil) composite materials to provide the required tribological properties. However, coatings consisting of nickel are extremely sensitive to sulfur; over time, coatings can be broken down when sulfur-containing gasoline is used [3]. Due to economic considerations, cylinder liners used in hypoeutectic Al-Si engine blocks are mostly cast iron. However, the use of cast iron liner causes some problems. The main problems can be summarized as follows. The bond between the cast iron liner and the cylinder block is only mechanical, no metallic bond; this makes the heat conduction difficult. The mismatch in coefficients of thermal expansion of Al-Si alloy and cast iron can cause deformation of the cylinder liner. Besides, cast iron liners bring about an increase in engine weight [3].

Functionally graded materials (FGMs) are an advanced composite type consisting of two or more phases. The gradual structure is formed through the changes in the composition and/or microstructure of the phases within the material in a specific direction. The graded structure reduces local stress concentration, thermal and residual stresses frequently encountered in conventional composites. The centrifugal casting method is one of the simplest methods so that functionally graded material manufacturing can be realized economically. The concentration of the reinforcing particles in the radial direction can be controlled by centrifugal casting. Thus, parts with better thermal dimensional stability and better wear resistance can be manufactured [4].

*Corresponding author. *Email address:* cemertek@cumhuriyet.edu.tr

Liew et al. [5] studied the thermomechanical behavior of functionally graded hollow circular cylinders. They observed that FGMs cannot expand freely in a steady temperature field, unlike homogeneous materials, and this can cause large stresses in FGMs. Also, thermal stresses in the functionally graded cylinder depend on more factors (non-uniform thermal conductivity and linear thermal expansion coefficient, etc.), dissimilar to its homogeneous counterparts, and it is more complicated to estimate. For all cases in this study, it was observed that hoop stress is the dominant stress.

Jabbari et al. [6] presented an analytical solution for the calculation of asymmetric thermal and mechanical stresses in a thick hollow cylinder made of functionally graded material. They designed a material having properties which are depending on the variable r (radius), and material properties were defined as power functions of r. They observed that the magnitude of the radial stress increased when *m* (power law index) was increased. In this study, it is presented that when $m < 1$, the hoop stress through the radius declined. Because the modulus of elasticity is an increasing function of the radius, the hoop stress increased along the radius, when $m > 1$. Obata and Noda [7] investigated the thermal stresses in a hollow sphere and a hollow circular cylinder made of functionally graded material. They presented that the values and distributions of the hoop stress and axial stress are similar. However, they observed that the distribution of the radial stress is different from them and the magnitude of it is lesser than theirs. Ekici et al. [8] studied the thermal stress behaviors of temperature-dependent functionally graded rectangular plates (FGRPs) using Finite Difference Method (FDM) and Finite Element Method (FEM). They presented that FEM and FDM analyses show very similar results with respect to strain, temperature, and normal stress component levels. In addition, they observed that the distribution characteristics of temperature, strain, displacement, and stress components are highly similar. However, they noted that there are quite differences between the displacement levels of FEM and FDM analyses. They concluded that the finite difference method, which does not lose importance for structures with linear geometry, gives better results than the finite element method. Zhang et al. [9] investigated the mechanical properties and microstructure of functionally graded cup-shaped specimens. The specimens were produced using a backward extrusion process during the semi-solid state of aluminum alloy (A390). They observed that the content of primary Si gradually increased from the upper region to the bottom region of the cup-shaped functionally graded samples, and the hardness values through the axis of the cup-shaped specimen gradually decreased from the bottom region to the upper region. They stated that during the wear test, the weight loss of the upper region is higher than that of the lower region because of the accumulation of numerous Si particles in the bottom region. Lin et al. [10] studied the effects of different process parameters on the particle distributions and the particle segregation ratio of in situ primary Si/Mg_2Si particles in Al-Si-Mg functionally graded tubes produced by centrifugal casting method. They observed that in the functionally graded tubes, many primary Si and Mg_2Si particles segregated in the inner layer, (reinforcement layer), whereas few particles segregated in the outer layer (un-reinforcement layer). They presented that the particle segregation ratios of k (ratio of the width of the reinforcement layer to distance from the inner wall to the outer wall) increased as pouring or mold temperatures increased, but decreased when the mold rotation rate increased. It is stated that when the pouring or mold temperatures or rotation rate were increased, the particle size of primary Si and primary Mg_2Si became smaller. They reported that the largest hardness of HRB 72–75 observed at the middle position of the reinforcement layer of the functionally graded tube.

Although there are many studies on thermal analysis of functionally graded materials in literature, such as those presented above, there are few studies examining thermal stresses in functionally graded cylinder liners and Al-Si based functionally graded materials. It is found that mechanical and microstructural characteristics of the functionally graded cylinder liners are frequently investigated in those studies.

For all these reasons, it was considered that the functionally graded cylinder liner made of Al-Si alloy would bring many benefits in practice. The cylinder liner, which can be manufactured by a centrifugal casting method, will be functionally graded. Since the density of silicon is lower than the density of aluminum, the concentration of silicon by the effect of centrifugal force will be maximum on the inner surface, and it will be minimal on the outer surface of the cylinder liner by gradually decreasing through the radial direction. When compared to cast iron cylinder liner, the functionally graded cylinder liner made of Al-Si alloy will provide the following advantages.

1-Reduction of engine weight due to low density,
2-Eliminating the problems arising from the mismatch in the coefficients of thermal expansion of the cast iron liner and the aluminum cylinder block,

3-Since the outer surface of the liner will have the same amount of silicon as the cylinder block will, functionally graded liners will be more compatible with the engine block and the wear resistance will increase due to the high silicon content on the inner surface of the cylinder liner.

Thanks to all these advantages, functional graded and ungraded cylinder liners made of Al-Si alloy were analyzed by finite element method and they were evaluated in this study.

2. Material and Methods

Recently, Al-Si alloys have been widely used in cylinder block manufacturing to reduce engine weight. Thus, Al-Si alloy was chosen as the material in this study. A319 and A356 aluminum alloys are the most commonly used materials in engine block manufacturing [1]. A356 aluminum alloy contains 6.5-7.5% (7.45-8.58% volume fraction) silicon. Therefore, the functionally graded cylinder liner was designed as having an outer surface containing 8.5 vol.% silicon to be compatible with engine block and an inner surface with 32 vol.% silicon for better wear resistance. The functionally graded cylinder liner (Fig. 1) was divided into twenty layers, each has a thickness of 0.3 mm. In the ungraded cylinder liner, which was designed for the comparison, the silicon distribution is homogeneous and the volume fraction of silicon is 21%. Cylinder liners were designed with a wall-thickness of 6 mm, an inner diameter of 74 mm, an outer diameter of 86 mm and a length of 165 mm.

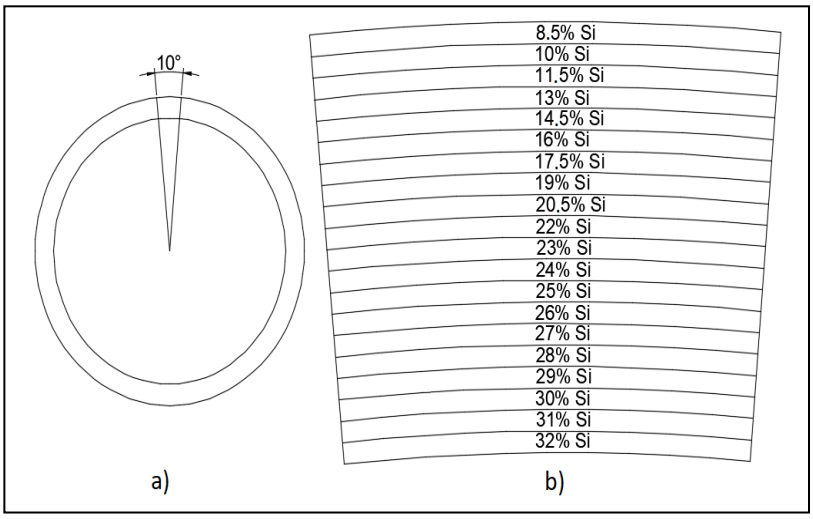

Figure 1. Functionally graded cylinder liner: (a) the entire liner; (b) 20 times magnified view of the 10 ° section, and the silicon content of the layers.

3. Determination Of Material Properties

In this study, the functionally graded cylinder liner has a twenty-layered structure. The silicon content of each layer (alloy) is distinct, so the material properties for each layer must be determined one by one.

3.1. Determination of mechanical properties

Mori-Tanaka method [11] was used to calculate the modulus of elasticity, shear modulus, bulk modulus and Poisson's ratio of the alloys.

The bulk modulus for each layer (alloy) was calculated by using an equation (1).

$$B_{Com} = B_{Al} + \frac{(B_{Si} - B_{Al}).v_{Si}}{1 + \frac{(1-v_{Si}).(B_{Si}-B_{Al})}{B_{Al}+\left(\frac{4}{3}\right).S_{Al}}} \quad (1)$$

Here, B_{Al} is the bulk modulus of aluminum, B_{Si} is the bulk modulus of silicon, S_{Al} is the shear modulus of aluminum and v_{Si} is the volume fraction of silicon in the alloy.

The shear modulus for each layer was calculated by using an equation (2).

$$S_{Com} = S_{Al} + \frac{(S_{Si} - S_{Al}).v_{Si}}{1 + \frac{(1-v_{Si}).(S_{Si}-S_{Al})}{S_{Al}+f_1}} \quad (2)$$

$$f_1 = \frac{S_{Al}.(9.B_{Al} + 8.S_{Al})}{6.(B_{Al} + 2.S_{Al})} \quad (3)$$

Here, S_{Si} is the shear modulus of silicon.

The density for each layer was calculated by using an equation (4).

$$d_{Com} = d_{Al}.v_{Al} + d_{Si}.v_{Si} \quad (4)$$

Here, d_{Al} is the density of aluminum, d_{Si} is the density of silicon, and v_{Al} is the volumetric fraction of aluminum in the alloy.

The Poisson's ratio for each layer was calculated by using an equation (5).

$$\nu_{Com} = \frac{1}{2.(1 + \frac{S_{Com}}{\lambda})} \quad (5)$$

$$\lambda = B_{Com} - \frac{2}{3}S_{Com} \quad (6)$$

The modulus of elasticity for each layer was calculated by using an equation (7).

$$E_{Com} = 3.(1 - 2.\nu_{Com}).B_{Com} \quad (7)$$

The modules of elasticity, Poisson's ratios and densities of aluminum and silicon at 25 °C are given in Table 1.

Table 1. Modulus of elasticity, Poisson's ratio and density of Al and Si elements at 25 °C [12,13].

	Elastic modulus (GPa)	Poisson's ratio	Density (kg/m^3)
Aluminum	70.2	0.345	2700
Silicon	162	0.22	2330

By using equations (8) and (9), bulk modulus and shear modulus of aluminum and silicon were calculated (Table 2)

$$B = \frac{E}{3(1-2\nu)} \quad (8)$$

$$S = \frac{E}{2(1+\nu)} \quad (9)$$

Table 2. Bulk modulus and shear modulus of Al and Si elements at 25 °C.

	Bulk modulus (GPa)	Shear modulus (GPa)
Aluminum	75.48	26.1
Silicon	96.4	66.4

To calculate the mechanical properties at different temperatures, Davoudi's study [14] was used, and Table 3 was formed.

Table 3. Shear modulus and Poisson's ratio of aluminum at 100 °C and 200 °C.

Temperature	Shear modulus (GPa)	Poisson's ratio
100 °C	25.076	0.349
200 °C	23.71	0.355

By using the equations (9) and (8), bulk modulus and modulus of elasticity of aluminum at 100 °C and 200 °C were calculated and presented in Table 4.

Table 4. Bulk modulus and modulus of elasticity of aluminum at 100 °C and 200 °C.

Temperature	Bulk modulus (GPa)	Modulus of elasticity (GPa)
100 °C	74.73	67.66
200 °C	74.1	64.274

Since the mechanical properties of silicon had little changes between 20 °C and 200 °C [15], the differences in mechanical properties of silicon were not included in the calculations.

For each Al-Si alloy (layer), the density at 25 °C was calculated by the equation (4), and mechanical properties at 25 °C, 100 °C and 200 °C were calculated using the equations (1), (2), (5) and (7). In addition, the elastic modules and the shear modules of the Al-Si alloys with various silicon content at 25 °C, 100 °C and 200 °C are given in Fig. 2 and Fig. 3.

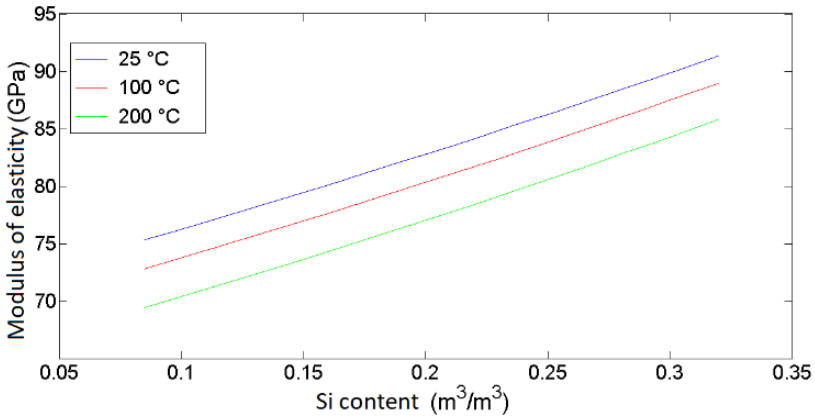

Figure 2. The elastic modules of Al-Si alloys with various silicon content at 25 °C, 100 °C and 200 °C.

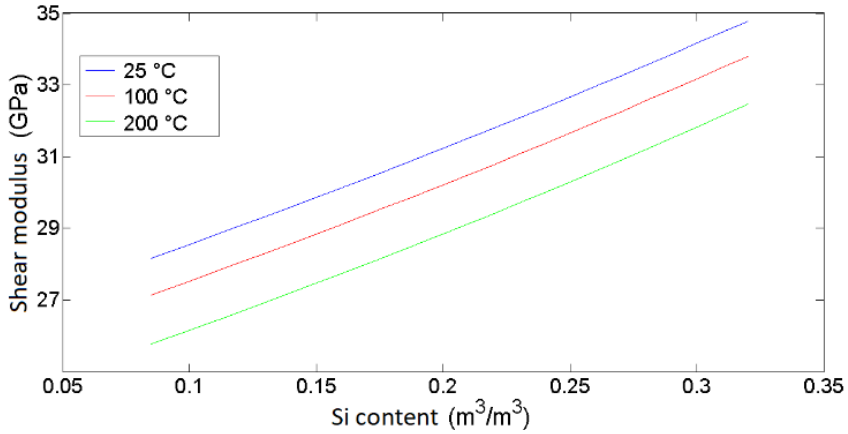

Figure 3. The shear modules of Al-Si alloys with various silicon content at 25 °C, 100 °C and 200 °C.

3.2. Determination of thermal properties

In the study by Huang et al., it was observed that the thermal expansion coefficients of Al-Si alloys obtained with an experimental method were very close to those calculated by using the Turner model [16]. Therefore, the Turner model [17] was used in this study to calculate the coefficients of thermal expansion of the Al-Si alloys, and the equation is shown below.

$$CTE_{Com} = (CTE_{Al} v_{Al} B_{Al} + CTE_{Si} v_{Si} B_{Si})/(v_{Al} B_{Al} + v_{Si} B_{Si}) \quad (10)$$

Here, CTE_{Al}, CTE_{Si} and CTE_{Com} are respectively the thermal expansion coefficient of aluminum, silicon and the Al-Si alloy.

The thermal expansion coefficients of aluminum and silicon at 20 °C, 100 °C and 200 °C are given in Table 5.

Table 5. Linear thermal expansion coefficients of aluminum and silicon at 20 °C, 100 ° and 200 °C [18-20].

	Linear thermal expansion coefficient (µm/m.°C)		
	20 °C	100 °C	200 °C
Aluminum	23	24.2	25.7
Silicon	2.5	3	3.4

The coefficients of thermal expansion at 20 °C, 100 °C and 200 °C were calculated for each Al-Si alloy (layer) by using the equation (10) and it is given in Fig. 4.

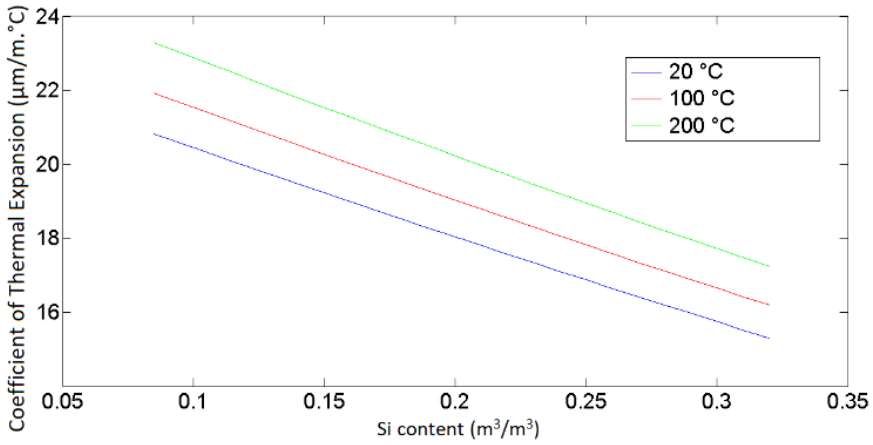

Figure 4. The thermal expansion coefficient of Al-Si alloy at 20 °C, 100 °C and 200 °C versus Si content.

The thermal conductivity coefficients of the Al-Si alloys at 25 °C with Si content of 8.5 vol.%, 15 vol.%, 20.5 vol.%, 30 vol.% and 45.5 vol.% were determined from the study of Sadatomi et al. [21], and are given in Table 6. The thermal conductivity coefficient was assumed to vary linearly between these values.

Table 6. Thermal conductivity coefficients of the Al-Si alloys.

Si content (m^3/m^3)	Coefficient of Thermal Conductivity (W/m. °C)
0.085	202.94
0.15	180
0.205	166.9
0.3	161.18
0.455	154.4

Every et al.'s study [22] was examined, and the thermal conductivity coefficients of the Al-Si alloys at different temperatures were calculated by using equations (11) and (12). The equation (11) was used for the Al-Si alloys having low silicon content (8.5 vol.%, 15 vol.% and 20.5 vol.%) and the equation (12) was used for the Al-Si alloys with high silicon content (30 vol.% and 45.5 vol.%).

$$\frac{K_{Com}}{K_{Al}} = \frac{[K_{Si}(1+2\alpha)+2K_{Al}]+2v_{Si}[K_{Si}(1-\alpha)-K_{Al}]}{[K_{Si}(1+2\alpha)+2K_{Al}]-v_{Si}[K_{Si}(1-\alpha)-K_{Al}]} \quad (11)$$

$$(1-v_{Si})^3 = \left\{\frac{K_{Al}}{K_{Com}}\right\}^{(1+2\alpha)/(1-\alpha)} \text{ x } \left\{\frac{K_{Com}-K_{Si}(1-\alpha)}{K_{Al}-K_{Si}(1-\alpha)}\right\}^{3/(1-\alpha)} \quad (12)$$

Here, K_{Al}, K_{Si} and K_{Com} are respectively the thermal conductivity coefficient of aluminum; silicon and Al-Si alloy.
Thermal conductivity coefficients of aluminum at 25 °C and silicon at 25 °C, 127 °C and 227 °C are given in Table 7.

Table 7. Thermal conductivity coefficients of aluminum and silicon [23-25].

	Coefficient of Thermal Conductivity (W/m. °C)		
	25 °C	127 °C	227 °C
Aluminum	235.2	232.3	229
Silicon	149	105	80

Since the thermal conductivity coefficient of aluminum slightly changes between 20 °C and 200 °C [23], the differences in the coefficients of thermal conductivity of aluminum were not taken into consideration in calculations.

The α values calculated by using the equations (11) and (12) which are given in Table 8.

Table 8. Calculated α values for different Si contents.

Si content (m^3/m^3)	0.085	0.15	0.205	0.3	0.455
α	-13.8613	-13.4757	-35	3.2995	1.0197

By substituting K_{Si} values at 127 °C and 227 °C and α values into equations (11) and (12), thermal conductivity coefficients at 127 °C and 227 °C were calculated for the Al-Si alloys having various silicon content (8.5 vol.%, 15 vol.%, 20.5 vol.%, 30 vol.% and 45.5 vol.%). It is assumed that the thermal conductivity coefficient has linear changes between these values. The calculated values for each alloy are shown in Table 9.

Table 9. Thermal conductivity coefficients of each Al-Si alloy at 25 °C, 127 °C and 227 °C.

Silicon content of Al-Si alloys (m^3/m^3)	Thermal conductivity coefficient (W/m. °C)		
	25 °C	127 °C	227 °C
0.085	202.940	202.730	202.480
0.1	197.646	197.399	197.108
0.115	192.352	192.068	191.735
0.13	187.058	186.738	186.363
0.145	181.765	181.407	180.991
0.16	177.618	177.305	176.942
0.175	174.045	173.816	173.555
0.19	170.473	170.328	170.167
0.205	166.900	166.840	166.780
0.21	166.599	166.417	166.254
0.22	165.997	165.571	165.201
0.23	165.395	164.724	164.148
0.24	164.793	163.878	163.096
0.25	164.191	163.032	162.043
0.26	163.588	162.185	160.991
0.27	162.986	161.339	159.938
0.28	162.384	160.493	158.885
0.29	161.782	159.646	157.833
0.3	161.180	158.800	156.780
0.31	160.743	157.839	155.465
0.32	160.305	156.879	154.150

4. Thermal Stress Analysis

ANSYS 17.1 Workbench software was used to determine the thermal stresses in the cylinder liners. First, steady state thermal analysis was performed to obtain three-dimensional temperature distribution of the liners.

A twenty-layered geometry consisting of the layers with a thickness of 0.3 mm and a length of 165 mm was formed by using the ANSYS Workbench for the functionally graded cylinder liner. A bonded connection was created between the layers. Then all material properties determined by using mathematical models and experimental data were entered into the program, and material assignment was realized for each layer. After that, a volumetric prismatic finite *element* mesh consisting of 193480 elements, was *generated.* Quadrilateral (3x3 mm) and triangular (0.3x3 mm) elements were used for cylindrical and flat surfaces, respectively. The generated finite element mesh is shown in Fig. 5 and Fig. 6.

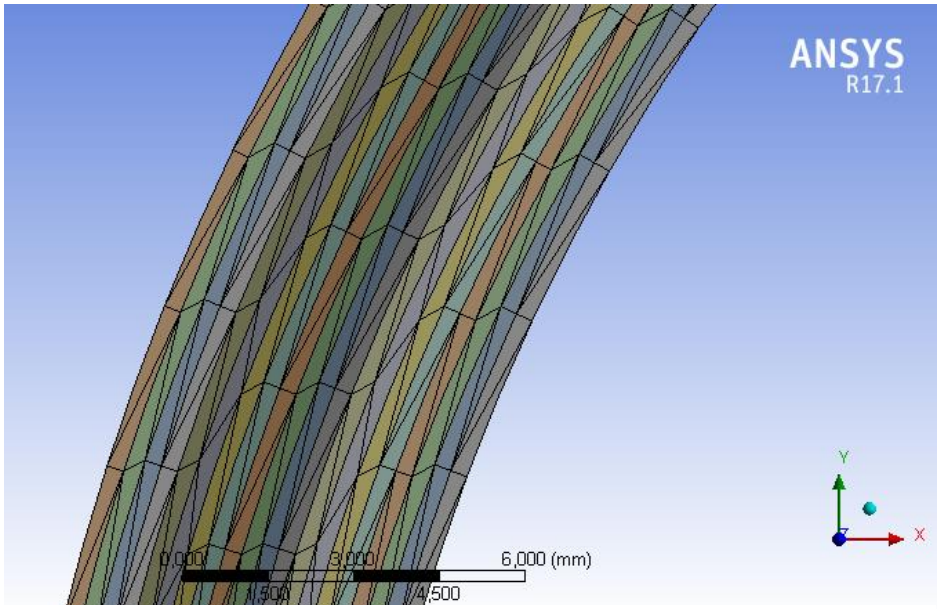

Figure 5. The finite element mesh on the flat surfaces of the functionally graded cylinder liner.

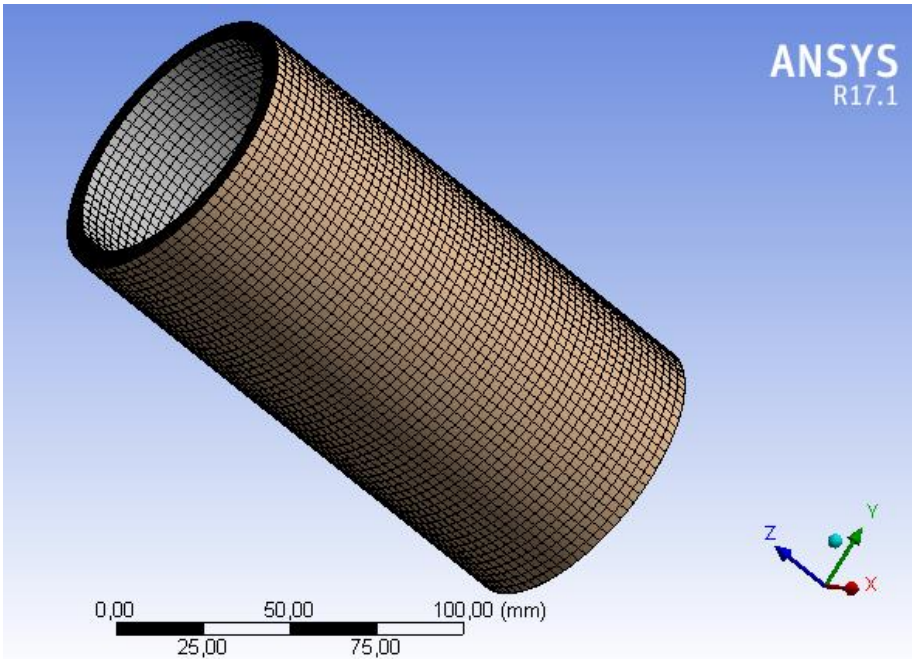

Figure 6. The finite element mesh of the functionally graded cylinder liner.

Wang et al. [26] studied three-dimensional temperature distribution in cylinders of a water-cooled gasoline engine by numerical methods. The average values obtained from this study were entered into the program as the final temperature values of the functionally graded cylinder liner. 180 °C, 120 °C, 110 °C and 85 °C, which were taken from the study of Wang et al., are the temperature values at the upper and lower edges of the inner surface and at the upper and lower edges of the outer surface of the cylinder liner, respectively. A model with an inner diameter of 74 mm, a thickness of 0.3 mm and a length of 165 mm was designed to find the temperature distribution on the inner surface of the liner. Al-Si alloy containing 32% Si was assigned as material for this model, and 180 °C and 120 °C temperature values were respectively entered into the program for the upper and lower surfaces of the model (Fig. 7(a)). The resulting temperature distribution is shown in Fig. 8(a).

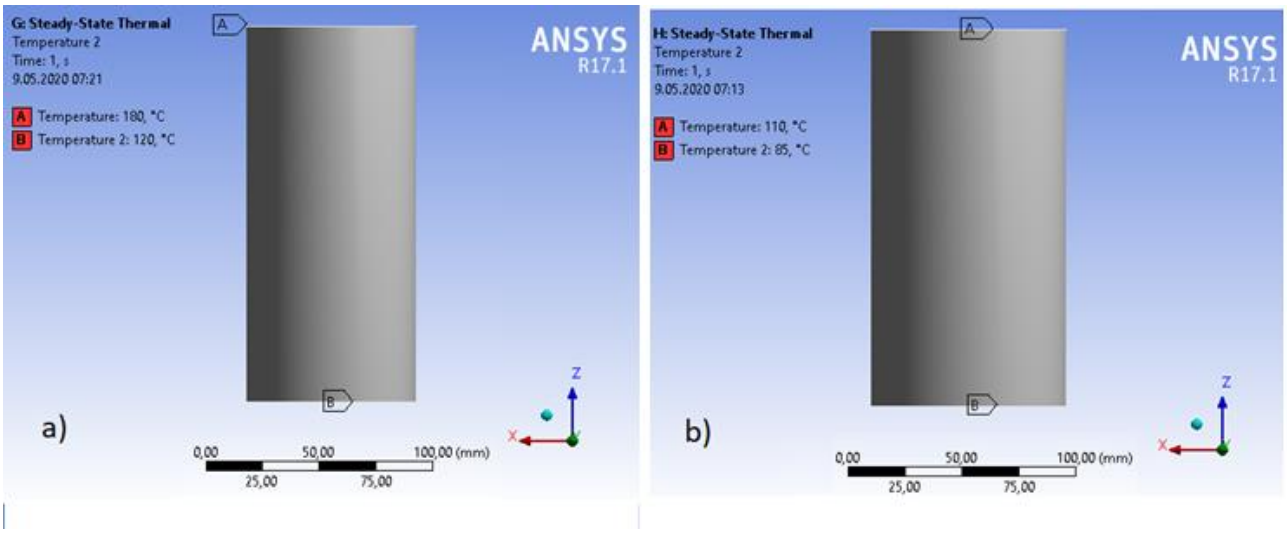

Figure 7. The boundary conditions for the steady-state thermal analysis of the functionally graded cylinder liner: (a) inner surface, (b) outer surface.

A model with an outer diameter of 86 mm, a thickness of 0.3 mm and a length of 165 mm was designed to find the temperature distribution on the outer surface of the functionally graded cylinder liner. Al-Si alloy with an 8.5 vol.% silicon content was assigned as material for this model, and 110 °C and 85 °C temperature values were respectively entered into the program for the upper and lower surfaces of the model (Fig. 7(b)). The temperature distribution on the outer surface of the cylinder liner is given in Fig. 8(b). The temperatures of inner and outer surfaces were taken into the functional graded model and three-dimensional temperature distribution was obtained (Fig. 8(c)).

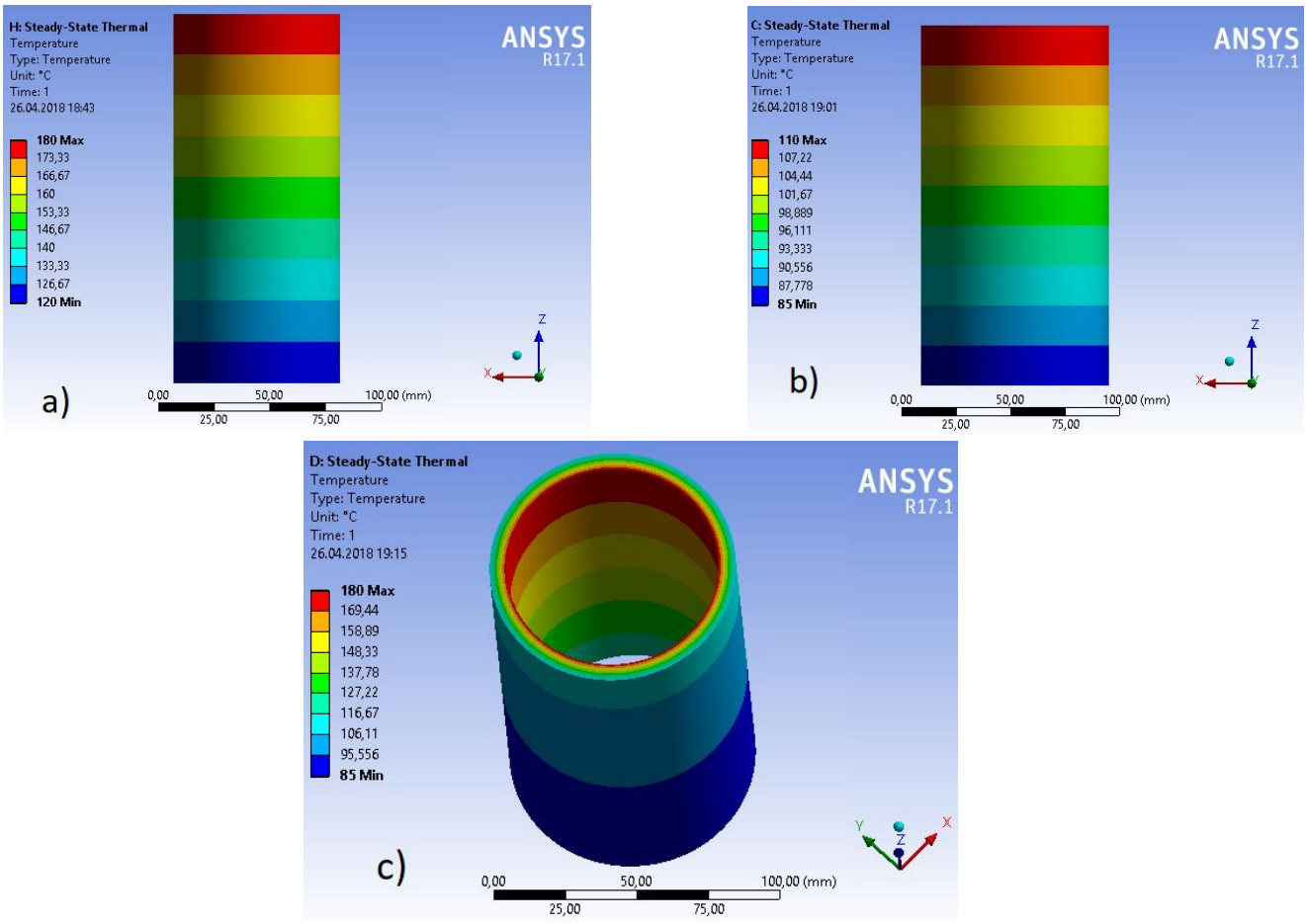

Figure 8. Temperature distribution of the functionally graded cylinder liner: (a) inner surface, (b) outer surface and (c) three-dimensional temperature distribution of the liner.

The temperature change through the thickness of the functionally graded cylinder liner is given in Fig. 9 and Fig. 10.

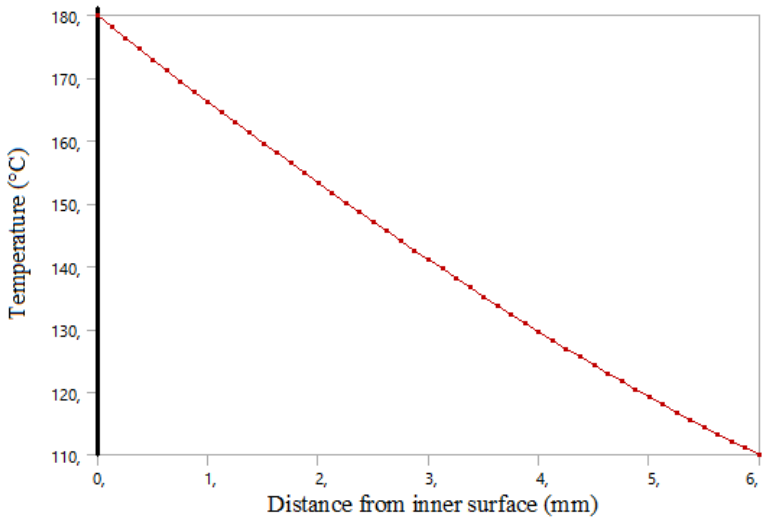

Figure 9. Temperature change through the thickness for the upper surface of the cylinder liner.

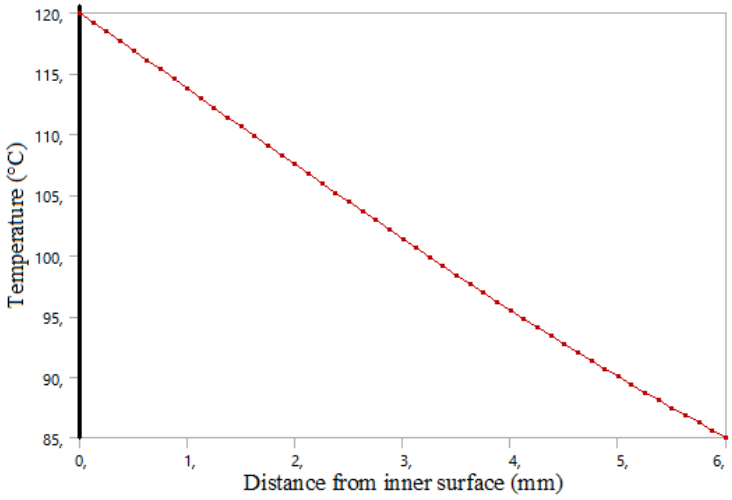

Figure 10. Temperature change through the thickness for the lower surface of the cylinder liner.

For the static structural analysis of the functionally graded cylinder liner, the same geometric model (twenty-layer) was used, and the same finite element mesh used in the thermal analysis was generated, only the element size was changed as 3.5 mm. The three-dimensional temperature distribution, which was obtained from the thermal analysis, was taken into the static analysis and it was applied as a thermal load. In statistical analysis, the ambient temperature entered into the program was 22 °C, and no constraints were applied. During the analysis, some weak springs were automatically applied by the program to restrain the rigid body motion.

The ungraded (homogeneous) cylinder liner with an inner diameter of 74 mm, an outer diameter of 86 mm and a length of 165 mm was designed for the comparison to the functionally graded cylinder liner.

In the thermal analysis, finite element mesh was generated with an average element size of 3mm by 3mm for the ungraded cylinder liner. Al-Si alloy containing 21% Si was assigned as material. The same of the boundary conditions applied to the functionally graded cylinder liner were applied and the three-dimensional temperature distribution of the ungraded cylinder liner (Fig. 11) was found.

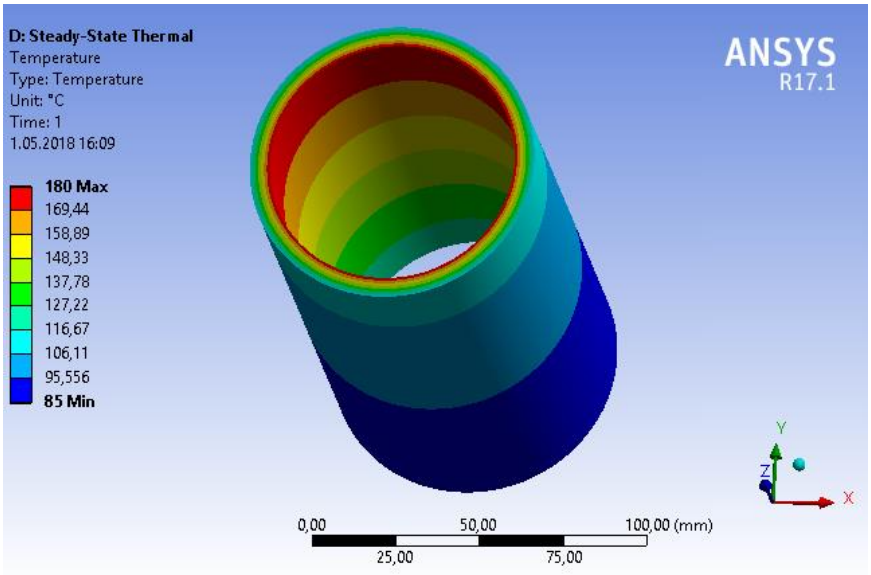

Figure 11. Three-dimensional temperature distribution of the ungraded (homogeneous) cylinder liner.

By respectively using quadrilateral (3.5x3.5 mm) and *t*riangular (0.3x3.5 mm) elements for the cylindrical and flat surfaces, a volumetric prismatic finite *element* mesh was *generated* in the statistical structural analysis of the ungraded cylinder liner. The three-dimensional temperature distribution of the ungraded cylinder liner was taken into the static structural analysis and applied as a thermal load. The same boundary conditions in the statistical structural analysis of the functionally graded cylinder liner were applied to the ungraded cylinder liner as well.Von Mises stresses in the functional graded and ungraded cylinder liners obtained from statistical analyzes are given in Fig. 12.

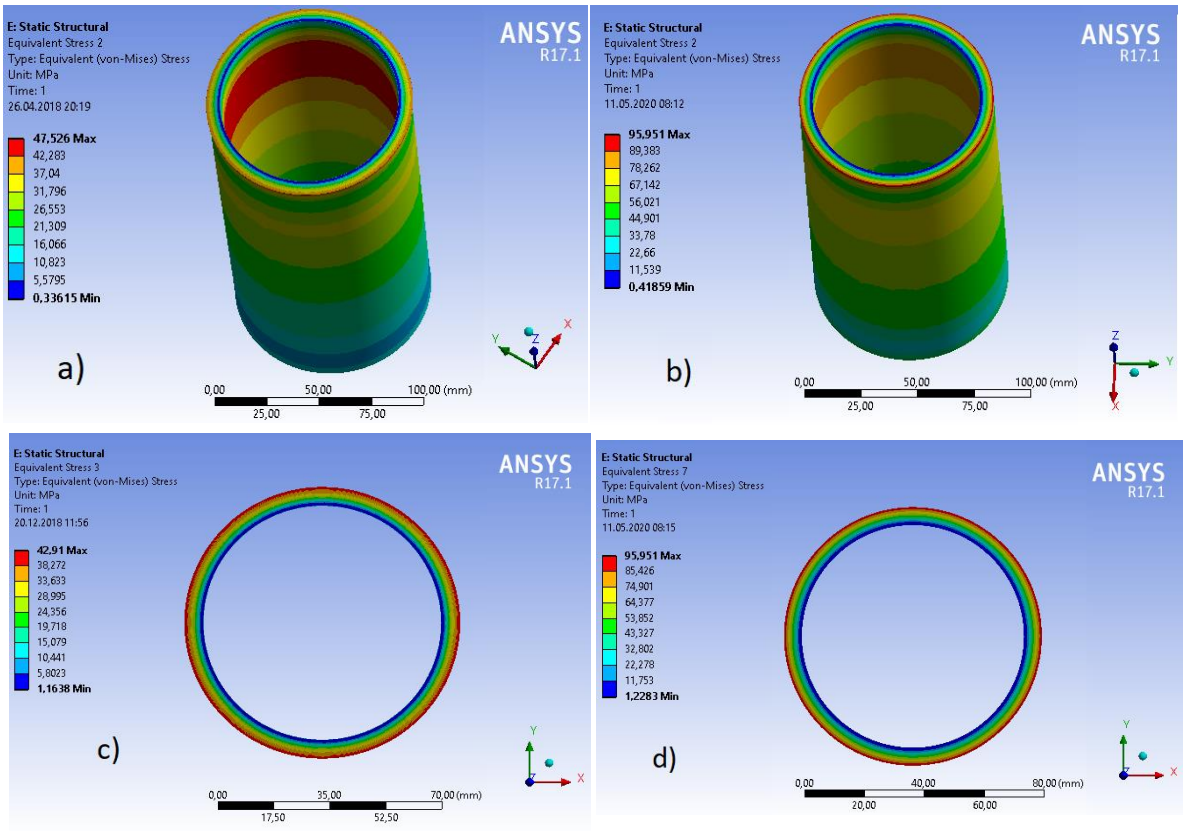

Figure 12. Von Mises stresses in the cylinder liners: (a) functionally graded cylinder liner, (b) ungraded cylinder liner, (c) the upper surface of the functionally graded cylinder liner, (d) the upper surface of the ungraded cylinder liner.

In addition, the statistical structural analysis of the functionally graded cylinder liner was performed by using elements with different sizes in order to see the effect of the element size on the results of the analysis. The maximum Von Mises stresses obtained from these analyses are presented in Table 10.

Table 10. Maximum Von Mises stresses in the functionally graded cylinder liner analyzed by using elements with different sizes.

Element Type	Element Size (mm)	Number of Finite Elements	Maximum Von Mises Stress (MPa)
Triangular Prism	3.5	147024	47.526
	5	76160	47.849
	6	53760	48.199

Table 10 shows that maximum Von Mises stress changed little when element sizes were increased. For instance, when the element size was increased from 3.5 mm to 5 mm, the maximum Von Mises stress increased by 0.68%.

In the literature, no similar study could be found to compare to our study since the results of the analysis vary greatly depending on cylinder liner dimensions, thermal load application, cylinder liner material and boundary conditions.

There are many studies in the literature presenting that thermal stresses are reduced in functionally graded materials. For example, in the study of Tahani [27], it is observed that temperature and thermal stress distributions are improved in the functionally graded shells compared to the classical layered composites.

In addition, Bako et al. [28] studied the simulation of a cast iron cylinder liner. In this study, the interior and the exterior temperatures of the cylinder liner were applied to be 2227 °C and 400 °C respectively, and the maximum compression pressure was applied to be 20 bar. They presented that the maximum Von Mises stress (21.08 MPa) occurred at the inner surface of the cylinder liner, and the minimum Von Mises stress (1.21 MPa) was observed at the outer surface of the cylinder liner. Abdalla et al. [29] investigated the thermo-mechanical stress behaviors in functionally graded (FG) rotating hollow disks with variable thickness. They designed a material as functionally graded in the radial direction. They assumed that materials properties vary along the radius according to a highly accepted power-law model. They designed four different structures: totally metal (TM), totally ceramic (TC), CM (inside is ceramic, outside is metal), and MC (inside is metal, outside is ceramic). The FG structures (MC and CM) were assumed to be a composition of steel and alumina. They assigned the inner and outer surface temperatures to be 300 °C and 100 °C, respectively. They stated that maximum and minimum Von Mises stresses were occurred in the MC and CM structures, respectively. The fact that the functionally graded material with CM structure exhibits the minimum Von Mises stress supports the results of our study.

5. Conclusion

The functionally graded cylinder liner, which can be manufactured by the centrifugal casting of Al-Si alloy containing 21 vol.% silicon, was designed with a silicon content of 32 vol.% on the internal surface and 8.5 vol.% Si on the outer surface. As for the ungraded cylinder liner, it is homogeneous and it contains 21% Si. The Cylinder liners were analyzed by using a finite element method, and the following results were obtained.

Considering the results obtained from the mathematical models and the previous researches in the literature, it was observed that the increase of silicon content in Al-Si alloys increased the modulus of elasticity of the alloy and decreased the thermal expansion and thermal conductivity coefficients. The temperature rises in the Al-Si alloys increased the coefficient of thermal expansion of the alloy but reduced the modulus of elasticity and thermal conductivity coefficient.

As a result of the applied thermal load, thermal stresses were observed in the functional graded and ungraded cylinder liners. The cause of the thermal stresses in the ungraded cylinder liner is the non-uniform temperature distribution. It is seen that not only the non-uniform temperature distribution is a reason for the thermal stresses in the functionally graded cylinder liner, but also it is the silicon content changing.

The maximum Von Mises stresses in the functionally graded and ungraded cylinder liners were determined to be 47.526 MPa and 95.951 MPa, respectively. The maximum Von Mises stress was reduced by approximately 50% due to the functionally grading. The temperature (between 180 °C and 120 °C) of the inner surface of the functionally graded cylinder liner is higher than the temperature (between 110 °C and 85 °C) of the outer surface. The increase of the Si content decreased the thermal expansion coefficient of the alloy. Since the thermal expansion is directly proportional to the product of the temperature difference and the coefficient of thermal expansion, the differences of thermal expansion between regions in the functionally graded cylinder liner are less than that in the ungraded cylinder liner. Therefore, the thermal stresses in the functionally graded cylinder liner are lower.

As a result of the analyses, it was found that the thermal stresses were lower in the functionally graded cylinder liner. Therefore, it is anticipated that the lifetime of the functionally graded cylinder liners will be longer than that of the ungraded liners.

Conflicts of interest

There is no conflict of interest.

References

[1] Ram S.C., Chattopadhyay K. and Chakrabarty I., High temperature tensile properties of centrifugally cast in-situ Al-Mg_2Si functionally graded composites for automotive cylinder block liners, *Journal of Alloys and Compounds*, 724 (2017) 84-97.

[2] Santos H.O., Costa I. and Rossi J. L., Mechanical and Microstructural Characterisation of Cylinder Liners, *Materials Science Forum*, 416 (2003) 407-412.

[3] Javidani M. and Larouche D., Application of Cast Al-Si Alloys in Internal Combustion Engine Components, *International Materials Reviews*, 59(3) (2014) 132-158.

[4] Jayakumar E., Jacob J.C., Rajan T.P.D., Joseph M.A. and Pai B.C., Processing and Characterization of Functionally Graded Aluminum (A319)-SiC_p Metallic Composites by Centrifugal Casting Technique, *Metallurgical and Materials Transactions A*, 47(8) (2016) 4306-4315.

[5] Liew K.M., Kitipornchai S., Zhang X.Z. and Lim C.W., Analysis of the thermal stress behaviour of functionally graded hollow circular cylinders, *International Journal of Solids and Structures*, 40(10) (2003) 2355–2380.

[6] Jabbari M., Sohrabpour S. and Eslami M.R., Mechanical and thermal stresses in a functionally graded hollow cylinder due to radially symmetric loads, *International Journal of Pressure Vessels and Piping*, 79(7) (2002) 493–497.

[7] Obata Y. and Noda N., Steady thermal stresses in a hollow circular cylinder and a hollow sphere of a functionally gradient material, *Journal of Thermal Stresses*, 17(3) (1994) 471-487.

[8] Demirbaş M.D., Ekici R. and Apalak M.K., Thermoelastic analysis of temperature-dependent functionally graded rectangular plates using finite element and finite difference methods, *Mechanics of Advanced Materials and Structures*, 27(9) (2020) 707-724.

[9] Zhang K., Yu H., Liu J., Li Y., Liu J. and Zhang J., Microstructure and property of a functionally graded aluminum silicon alloy fabricated by semi-solid backward extrusion process, *Materials Science & Engineering A*, 624 (2015) 229-238.

[10] Lin X., Liu C. and Xiao H., Fabrication of Al–Si–Mg functionally graded materials tube reinforced with in situ Si/Mg2Si particles by centrifugal casting, *Composites: Part B*, 45(1) (2013) 8-21.

[11] Saunders W. L., Pendley K. and Gutierrez-Miravete E., Modal analysis of functionally graded metal-ceramic composite plates, Proceedings of the 2014 COMSOL Conference, 8-10 October, Boston, (2014).

[12] Cardarelli F., Background Data for the Chemical Elements. In: Materials Handbook: A Concise Desktop Reference. 2nd ed. London: Springer, 2008; pp 1181-1194.

[13] Lasagni F. and Degischer H.P., Enhanced Young's Modulus of Al-Si Alloys and Reinforced Matrices by Co-continuous Structures, *Journal of Composite Materials*, 44(6) (2010) 739-755.

[14] Davoudi K., Temperature dependence of the yield strength of aluminum thin films: Multiscale modeling approach, *Scripta Materialia*, 131 (2017) 63-66.

[15] Kahn H., Huff M.A. and Heuer A.H., Heating Effects on the Young's Modulus of Films Sputtered onto Micromachined Resonators, Proceedings, Microelectromechanical Structures for Materials Research, Materials Research Society Symposium 518, 15-16 April, San Franscisco, (1998) 33-38.

[16] Ma P., Jia Y., Prashanth K.G., Yu Z., Li C., Zhao J., Yang S. and Huang L., Effect of Si content on the microstructure and properties of Al–Si alloys fabricated using hot extrusion, *Journal of Materials Research*, 32(11) (2017) 2210-2217.

[17] Ibrahim I.A., Mohamed F.A. and Lavernia E.J., Particulate reinforced metal matrix composites - a review, *Journal of Materials Science*, 26(5) (1991) 1137–1156.

[18] Frank W.B., Koch G.P. and Mills J.J., Properties of Pure Aluminum. In: Hatch J.E., (Eds). Aluminum Properties and Physical Metallurgy. Ohio: American Society for Metals, 1984; pp 1-24.

[19] Jia Y.D., Ma P., Prashanth K.G., Wang G., Yi J., Scudino S., Cao F.Y., Sun J.F. and Eckert J., Microstructure and thermal expansion behavior of Al-50Si synthesized by selective laser melting, *Journal of Alloys and Compounds*, 699 (2017) 548-553.

[20] Kempe V., First-level Packaging. In: Inertial MEMS: Principles and Practice. New York: Cambridge University Press, 2011; pp 205-225.

[21] Sadatomi N., Hamamoto N., Saigo T. and Yamashita O., Thermal Characterization of Al-Si Materials Prepared by Die Casting Method, *Journal of the Japan Society of Powder and Powder Metallurgy*, 49(9) (2002) 793-798.

[22] Every A.G., Tzou Y., Hasselman D.P.H. and Raj R., The effect of particle size on the thermal conductivity of ZnS/diamond composites, *Acta Metallurgica et Materialia*, 40(1) (1992) 123-129.

[23] Jia Y., Cao F., Ma P., Scudino S., Eckert J., Sun J. and Wang G., Microstructure and thermal conductivity of hypereutectic Al-high Si produced by casting and spray deposition, *Journal of Materials Research*, 31(19) (2016) 2948-2955.

[24] Xiu Z., Chen G., Yang W., Song M. and Wu G., Microstructure and thermal properties of recyclable Si_p/1199Al composites, *Transactions of Nonferrous Metals Society of China*, 19(6) (2009) 1440-1443.

[25] Masolin A., Bouchard P., Martini R. and Bernacki M., Thermo-mechanical and fracture properties in single-crystal silicon, *Journal of Materials Science*, 48(3) (2013) 979-988.

[26] Wang G., Chen H., Yuan Z. and Lu W., Numerical Study on Three-Dimensional Steady-State Temperature Field of a Gasoline Engine, *Advanced Materials Research*, 569 (2012) 610-614.

[27] Tahani M., Analysis of functionally graded cylindrical shells subjected to mechanical and thermal loadings, Proceedings, 12th European conference on composite materials, 29th August-1st September, Biarritz, (2006).

[28] Bako S., Usman T., Bori I. and Nasir A., Simulation of a Wet Cylinder Liner, *SSRG International Journal of Mechanical Engineering*, 6(4) (2019) 12-17.

[29] Abdalla H.M.A., Casagrande D. and Moro L., Thermo-mechanical analysis and optimization of functionally graded rotating disks, *The Journal of Strain Analysis for Engineering Design*, (2020).